J Mater Sci: Mater Med (2009) 20:1031–1038
DOI 10.1007/s10856-008-3664-2

Preparation and characterization of nano-hydroxyapatite/polyamide 66 composite GBR membrane with asymmetric porous structure

Jidong Li · Yi Zuo · Xianmiao Cheng · Weihu Yang · Huanan Wang · Yubao Li

Received: 11 January 2008 / Accepted: 8 December 2008 / Published online: 30 December 2008

Abstract In this study, a nano-hydroxyapatite/polyamide 66 (nHA/PA66) composite with good biocompatibility and high bioactivity is employed to develop novel asymmetric structure porous membranes for guided bone regeneration (GBR). FT-IR and XRD analyses suggest that chemical bonds are formed between nHA and PA66 both in composite powders and membranes. The fabricated membranes show gradient porous structure. SEM analysis reveal that pores less than 10 μm and pores with a size ranging from 30 μm to 200 μm distribute in the micropore layer and the spongy structure layer, respectively. The surface energy determination also reveals that the fabricated membranes have asymmetric surface properties on the two sides of the membrane. The incorporation of nHA in PA66 matrix improves the properties of the membrane. The elongation at break and the tensile strength of nHA/PA66-40 suggest that the composite membrane has good strength and toughness. The rough porous structure surface with high surface energy of nHA/PA66 composite membrane may be beneficial to promote cells immobility and differentiation into a mature phenotype producing mineralized matrix. The biocompatibility, bioactivity, osteoconductivity, asymmetric porous structure, mechanical properties and hydrophilicity of the composite membrane can meet the requirement of GBR technique.

J. Li · Y. Zuo · X. Cheng · W. Yang · H. Wang · Y. Li (✉)
Research Center for Nano-Biomaterials, Analytical and Testing Center, Sichuan University, Chengdu 610064, China
e-mail: nic7504@scu.edu.cn

J. Li
e-mail: blueljd@163.com

1 Introduction

Guided tissue regeneration (GTR) is such a treatment that repairs tissue defect or reconstructs new tissue by using a barrier membrane to guard the defect site from invasion of other tissue, especially fibrous connective tissue [1]. GTR technique by using barrier membranes has been proved to be an effective modality in periodontal therapy [2–5]. The membrane offers protection so that mesenchymal stem cells can migrate without hindrance from the surrounding periodontium, permitting the formation of new periodontal tissue, especially progenitor bone and periodental ligament [6].

The barrier membrane technique was employed to guide bone regeneration in the bone defect site and proposed the term of "Guided bone regeneration (GBR)" by some researchers [7, 8]. Some properties of the barrier membrane are required in GTR or GBR process, such as excellent biocompatibility, suitable mechanical strength, mechanical stability and optimal porosity and so on. Porous structure both at the surface and sublayer of the membrane is essential for the cellular adaptation and sufficient nutrients permeation [9]. The advantage of asymmetric porous membranes for GTR or GBR was stated elsewhere [1, 10]. Briefly, in GBR process, the membranes cover on bone defect and the dense or less porous outer layer can prevent the ingrowth of fibrous connective tissue into defect area and the inner porous surface can enable cells, such as osteoblasts and mesenchymal stem cells, to colonize it to promote the bone regeneration. Rough surfaces also appear to promote immobility and differentiation of osteoblast into a mature phenotype producing mineralized matrix [11, 12].

In the past twenty years, non-absorbable and absorbable membranes had been studied and applied to GTR or GBR techniques. Non-absorbable membranes used currently

include expanded polytetrafluoroethylene (e-PTFE) [13–15], titanium and ethyl cellulose membranes [16]. However, non-biodegradable membranes such as e-PTFE required secondary surgical procedure for retrieval and this remained a significant drawback [15]. Absorbable membranes, such as chitosan [1], PLGA [12] and collagen [13, 17] membranes, have been received high interest in studies and clinical applications. The low mechanical strength, unstable properties and combination with bone graft always required of absorbable membranes effect the efficiency of GBR. Some reports suggested that better bone regeneration effect was obtained by using non-absorbable membrane in comparison with absorbable membrane for GBR [16, 18, 19]. Both the absorbable and non-absorbable barrier membranes have their shortcoming and the available products are limited. In order to overcome the drawbacks of the GBR membranes used currently and provide an optimal alternative, novel barrier membranes with multifunction need to be developed.

nHA/PA66 composite developed by our research group is a biomimetic and bioactive material using for bone repair engineering [20]. In nHA/PA66 composite, nHA particles can remain their nano-scale crystals and disperse uniformly in PA66 matrix and the nHA content can reach to 65 wt% in the composite. The composition, structure and mechanical properties of nHA/PA66 composite are similar to those of natural bone, which is responsible for good biocompatibility, osteoconductivity and bioactivity of the composite [21–23]. At present study, nHA/PA66 composite is employed to fabricate a novel bioactive barrier membrane with asymmetric porous structure by using phase inversion method. The good biocompatibility and osteoconductivity of the composite membrane are granted by the incorporation of nHA, and the toughness of the membrane is administrated via the continuous polymer phase of PA66. The membrane can be expected to prevent connective tissue migration into bony defect site and to promote growth of progenitor bone. Meanwhile, it has not to be removed by secondary surgical procedure due to the direct bonding with the surrounding host and/or regenerated bone. The composition, structure, mechanical strength and surface energy are also investigated and the results indicate that the composite membrane is suitable for GBR, including guided dental tissue regeneration.

2 Materials and methods

2.1 Preparation of nHA/PA66 composite slurry

PA66 with a viscosity-average molecular weight (Mv) of 18 kDa was from BASF, Germany. The slurry of nano-hydroxyapatite (nHA) used for composite was prepared by our laboratory. The nHA/PA66 composite slurry was prepared according to ref. [23]. PA66 was completely dissolved in ethanol solution at the temperature of 70°C. Then nHA slurry was gradually added into the PA66/ethanol solution with vigorously stirring for 2 h. nHA/PA66 composites with 40 wt% and 60 wt% of nHA were obtained separately. The abbreviation of the composites used through this paper can be explained as the example of nHA/PA66–40 and nHA/PA66-60, which 40 and 60 indicate the nHA weight percentage in the composites.

2.2 Membrane fabrication

The composite slurry was set for at least 4 h at room temperature to remove the bubble. Then the slurry was casted onto glass plate and spread slowly to form an even liquid film, then the liquid film was vaporized at room temperature for 48 h to form a membrane. Subsequently, the obtained membrane was washed repeatedly with deionized water. Pure PA66 membrane was also prepared by using pure PA66 slurry through the above-mentioned method.

2.3 Membrane characterization

Transmission IR spectra were recorded using a Nicolet 5700 Fourier transform infrared (FT-IR) spectrophotometer. Samples in powder form were mixed with KBr powder at 1/99 ratio and pressed into disk for spectra collection. Attenuated Total Reflectance (ATR) spectra of the membranes were also collected.

X-ray diffraction (XRD, Philips, X' Pert Pro, Cu Kα) was used to characterize the crystal structure of the materials both in powder and membrane form. Parts of the composites slurry were fully washed by deionized water, then dried and milled into powder for transmission IR spectra collection and XRD test. The PA66 particles were also milled into powder for transmission IR and XRD spectra collection.

The morphology of the membrane was observed by scanning electronic microscopy (SEM). The membranes were carefully sectioned with a razor blade and mounted onto copper stubs. Prior to examination, each sample was coated with gold. A Hitachi S-450 SEM microscope at 20 kV was used to perform image analysis.

Tensile strength and elongation at break were evaluated by using a Shimadzu AG-10TA electronic universal testing machine (Japan) and the average values of each membrane from at least five tests were reported. The swollen membranes were stamped out to dumbbell test pieces (about 0.3 mm in thickness, 6 mm in width and 20 mm in gauge length) and tested at a speed of 10 mm/min at 23°C and 65% RH. Tensile strength (*TS*) and elongation at break (*%E*) were calculated as follows:

$$TS = \frac{Fm}{A} \times 10^{-6} \text{ MPa} \quad (1)$$

where Fm = maximum loaded force (N) and A = cross-sectional area of samples (m^2).

$$\%E = \frac{\Delta L}{L_0} \times 100 \quad (2)$$

where ΔL = increase in gauge length at breaking point (mm) and L_0 = original gauge length (mm).

The surface energy of the membranes was also investigated through contact angle test by sessile drop method and calculated by harmonic mean method (Wu) [24] (Krüss DSA100, Germany). Water and diiodomethane were employed as polar and apolar testing liquid, respectively. Drops of 3 μl were used to determine static contact angle (at least 3–4 measurements per liquid) and calculate surface energies. The e-PTFE membrane used as control was supplied by Shanghai Plastics Research Institute.

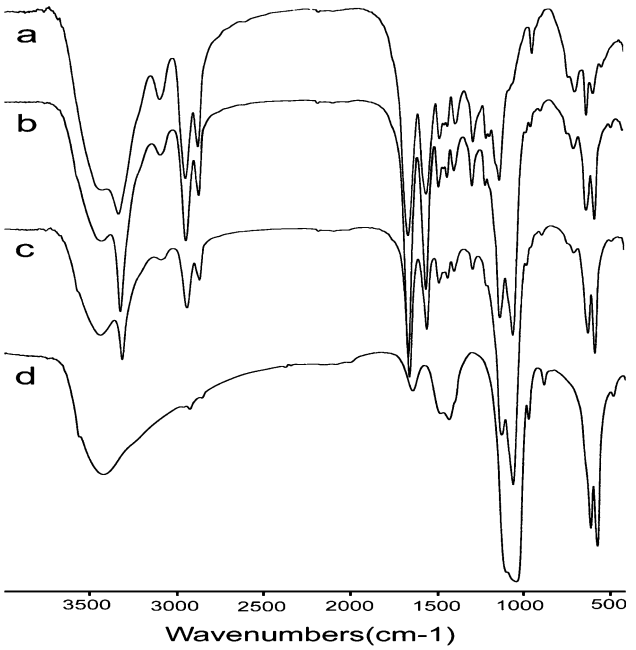

Fig. 1 IR spectra of PA66 (a), nHA/PA66-40 (b), nHA/PA66-60 (c) and nHA (d) powders

3 Results and discussion

3.1 IR analysis

The interaction between PA66 and hydroxyapatite (HA) can be formed via chemical bond because both PA66 and HA are polar compounds. The FT-IR spectra of PA66 (a), nHA/PA66-40 (b), nHA/PA66-60 (c) and nHA (d) in powder form are shown in Fig. 1 and the wavenumbers of the corresponding characteristic groups of the materials are listed in Table 1. It can be seen from Table 1, although the absorption peaks of nHA at 604 and 1,104 cm^{-1} move to high wavenumber due to the overlapping with the absorption peaks ascribed to PA66 of nHA/PA66-40 composite, the wavenumbers of others peaks of PO_4^{3-} have no significant change in the composites compared to that of pure nHA, suggesting that there is almost no chemical bond formed between PO_4^{3-} of nHA and PA66. The CO_3^{2-} peak located at 872 cm^{-1} in nHA moves to 867 cm^{-1} in the composites indicating that the nHA used is B-type carbonate substituted HA(some CO_3^{2-} ions replace some PO_4^{3-} ions) [25–27] and its chemical environment has changed after incorporation into the composites. The intensity reduction of carbonate absorption from Fig. 1d to Fig. 1c and Fig. 1b possibly results from the formation of chemical bond between CO_3^{2-} and PA66 or from the loss of CO_3^{2-} in the procedure of compounding nHA with PA66.

The OH^- vibration wavenumber (Table 1) and intensity (Fig. 1) of nHA are lower in composites than that of pure HA, indicating the hydrogen-bonds formed between OH^- of nHA and polyamide in the composites. In comparison of IR spectra of pure PA66 with that of PA66 in the composites, it is found that the stretching vibration wavenumber of carbonyl in polyamide hardly changes before and after compounding. However, the stretching vibration wavenumber of N–H has changed after compounding. The fact indicates that the hydrogen bonds mainly exist between OH^- of HA and amido of PA66, instead of carbonyl, because the π bonds between oxygen and carbon will weaken the electronegativity of oxygen in carbonyl, it is difficult to form hydrogen bonds for oxygen atom of carbonyl [23].

IR-ATR spectra of PA66, nHA/PA66-40 and nHA/PA66-60 membranes are shown in Fig. 2. The bands at approximately 1,091 and 1,032 cm^{-1} belong to the P–O vibration of nHA in Fig. 1b, c. The band at approximately 3,301 cm^{-1} should be attributed to N–H and the band at 1,636 cm^{-1} to C=O stretching vibration. The latter two vibrations strongly depend on hydrogen bond interactions between the PA66 chains [28]. The vibrations associated with C–H stretching (region between 2,800 and 3,000 cm^{-1}) also appear in both spectra. The N–H and C–O stretching vibrations in IR spectra of PA66 and nHA/PA66 composite membranes are similar, suggesting that the composition and structure of PA66 have not changed greatly after the incorporation of nHA. The intensity of P–O vibration absorption peaks is stronger in nHA/PA66-60 membrane than that in nHA/PA66-40 membrane.

Table 1 The wavenumbers (cm^{-1}) of PA66, nHA/PA66-40, nHA/PA66-60 and nHA

	Characteristic groups vibration	nHA	PA66	nHA/PA66-40	nHA/PA66-60
nHA	–OH	3,572	–	3,565	3,564
	PO_4^{3-}	1,036	–	1,034	1,035
		1,104	–	1,111	1,104
		567	–	566	566
		604	–	614	606
	CO_3^{2-}	872	–	867	867
PA66	N–H streching	–	3,310	3,304	3,303
	N–H bending	–	1,539	1,539	1,538
		–	685	687	691
	C=O streching	–	1,640	1,639	1,638
	$–CH_2–$ streching	–	2,927	2,931	2,930
	–CH– streching	–	2,858	2,859	2,858

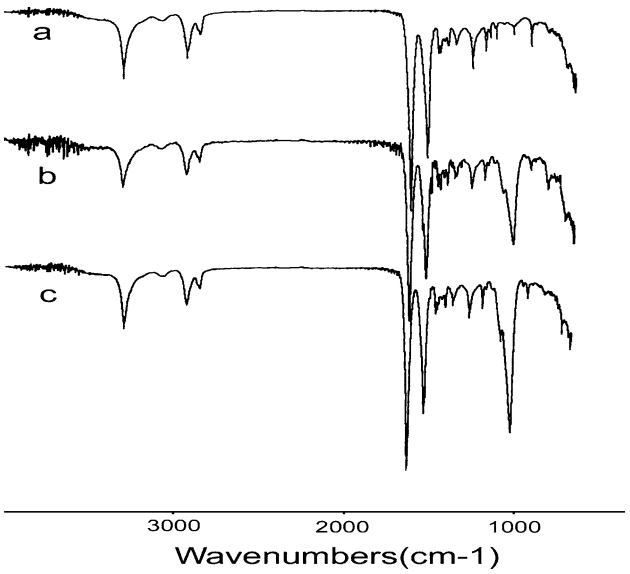

Fig. 2 IR (ATR) spectra of PA66 (a), nHA/PA66-40 (b) and nHA/PA66-60 (c) membranes

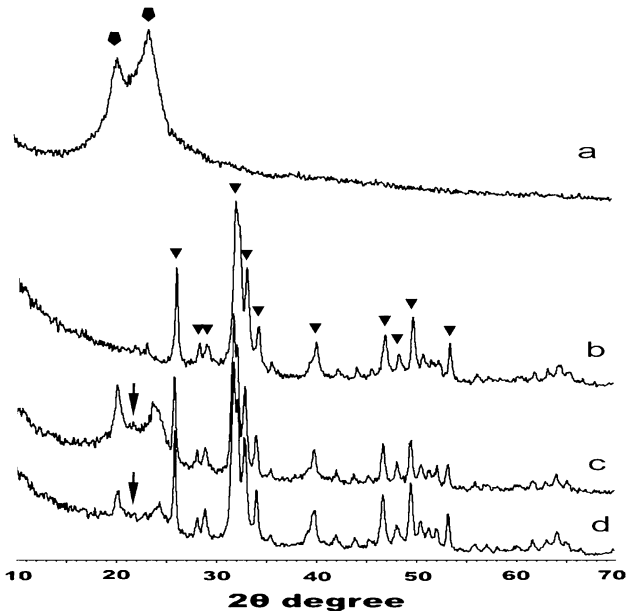

Fig. 3 XRD patterns of PA66 (a), nHA (b), nHA/PA66-40 (c) and nHA/PA66-60 (d) in powder. The characteristic peaks ascribed to nHA (▼), α phase (■) and γ phase (⬇) to PA66

3.2 XRD analysis

Figure 3 and Fig. 4 show the XRD patterns of PA66, nHA, nHA/PA66-40 and nHA/PA66-60 in powder and in membrane form, respectively. PA66 has various crystalline phases and usually presents the more stable α phase rather than the γ phase in XRD pattern. The two strong diffraction peaks at $2\theta \approx 20.4$ and 24.1° are the distinctive feature of α phase of PA66, which are designated as α1 and α2, respectively. The diffraction peak of the γ phase is at $2\theta \approx 21.8°$, the diffraction peak at $2\theta \approx 13.6°$ is also contributed by the γ phase, and they are designated as γ1 and γ2, respectively [29]. It can be seen from Figs. 3 and 4, almost all the characteristic peaks of HA appear both in the composite powders and in the composite membranes, while the intensity of these peaks decreases with the increase of weight percentage of PA66.

Though the intensities are lower than those of pure PA66, α1 and α2 are still the main diffraction peaks observed in the composite samples and γ phase also appear in the composite powders and membranes. We can draw the following conclusion from above results: the introduction of nHA induces the appearance of the γ phase in composites which is unstable and seldom appears in PA66 at room temperature, more nHA loadings would amplify this phenomenon; the addition of nHA also changes the structure of the α crystalline phase.

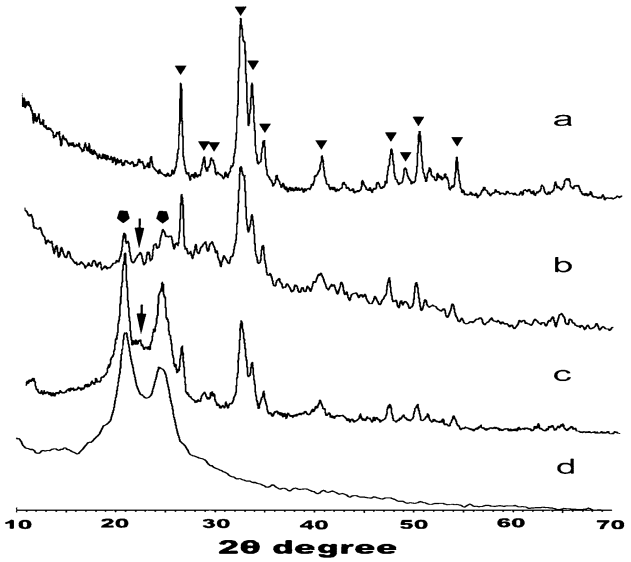

Fig. 4 XRD patterns of nHA (a) in powder, nHA/PA66-60 (b), nHA/PA66-40 (c) and PA66 (d) in membranes. The characteristic peaks ascribed to HA (▼), α phase (■) and γ phase (⏚) of PA66

Crystal sizes of nHA are calculated by Sherre formula from XRD patterns of different specimens [30]:

$$D_{hld} = \frac{0.89\lambda}{\sqrt{b^2 - b_0^2}\cos\theta} \quad (3)$$

where λ stands for wavelength, θ stands for Bragg angle, b stands for half width of the characteristic peak, and b_0 is the half width of XRD machine proof read by multicrystal silicon powder, giving a value of $b_0 = 0.1215$. Table 2 shows the crystal value calculated by the half width and Bragg angle of HA at its characteristic peaks: (002) peak and (300) peak. The data indicate that the size of HA crystals is in nanoscale and the size of HA crystals is bigger in composite than pure HA. This may be attributed to the influence of the process of composite preparation or/and the interaction between HA and PA66.

Index of crystallizable perfection (ICP) expresses the slight change of crystal unit volume along the axis orientation of the molecule. The ICP values of PA66 increase both in the composite powders and in the composite membranes compared to the pure PA66 (Table 3). The reason is that nHA in PA66 matrix plays a role of nucleating agent and enhances the crystallization process.

Table 2 The crystal size of nHA in the powder materials

	D(hkl) (nm)	Pure nHA	nHA/PA66-40	nHA/PA66-60
nHA	D(002)	33.4	38.2	37.3
	D(300)	13.4	16.8	15.6

Table 3 The ICP of PA66 in the powders and membranes

	Pure PA66	nHA/PA66-40	nHA/PA66-60
In powder	0.597	0.666	0.727
In membrane	0.599	0.668	0.685

3.3 Microstructure of the membranes

The purpose of membrane for GBR is to prevent apical migration of gingival epithelial cells into bony defect site and promote the growth of progenitor bone and periodontal ligament cells. The barrier membrane with asymmetric structure can meet the requirement of GBR. Therefore, porous structure both at the surface and sublayer of the membranes is essential for cellular adaptation and the permeation of sufficient nutrients [1]. The bilayer structure of Bio-Gide® membrane shows a compact, dense outer surface that prevents the ingrowth of fibrous connective tissue in vivo. The inner porous surface enables cells such as osteoblasts to colonize it [10]. Smooth surfaces promote osteoblast proliferation and migration while rough surfaces appear to promote immobility and differentiation into a mature phenotype producing mineralized matrix [11, 12].

Figure 5 shows the microstructure of PA66 (a, d, g), nHA/PA66-40(b, e, h, i) and nHA/PA66-60 (c, f) membranes observed by SEM. The cross section (Fig. 5i) of the fabricated membranes showed gradient porous structure, which the size of pores increasing gradually from the micropore layer to the spongy layer. The pores less than 10 μm distributed on the micropore surface (Fig. 5a–c) of the membranes, to prevent the fibrous connective tissue migration into bony defect site and promote growth of progenitor bone and permeate sufficient nutrients simultaneously. Fig. 5d–f show the spongy structure of the three types of membranes with the pore size ranging from 30 μm to 200 μm, which is often required for cell penetration and resulted in bonding with the original or regenerated tissue directly [31]. Figure 5g, h presents lots of small pores on the wall of the large pores. The interconnective porous structure has advantage for sufficient nutrients permeation, tissue regeneration and direct bonding between materials and tissues. Therefore, the architecture of the membrane can meet the requirement of GBR technique.

The shape of pores and surface roughness of PA66 membrane are different from those of the composite membranes. Both the surface and the wall of the pores of PA66 membrane are smooth, while the surface and the wall of the pores of the composite membranes are rougher than that of PA66 membrane (Fig. 5). The good biocompatibility, bioactivity and osteoconductivity of composite membranes result from the high content of nHA in the composites and the rough spongy surface can promote the

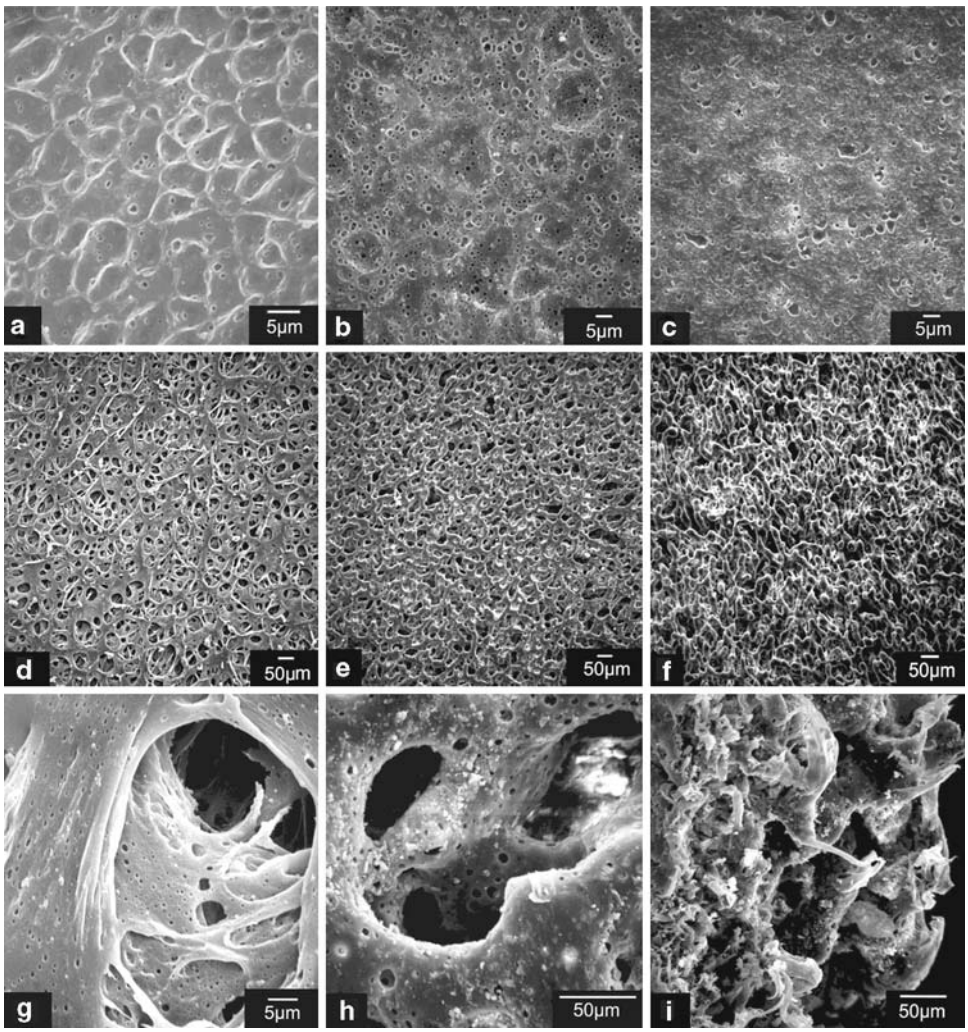

Fig. 5 SEM photos of the membranes: micropore surface of PA66 **a**, nHA/PA66-40 **b** and nHA/PA66-60 **c** membranes; porous surface of PA66 **d**, nHA/PA66-40 **e** and nHA/PA66-60 **f** membranes; the micropores located on the pore walls of macropores in the porous surface of PA66 **g** and nHA/PA66-40 **h** membranes; the cross-section of nHA/PA66-40 membrane **i**

bone formation through increased osteoblasts attachment, immobility and differentiation into a mature phenotype producing mineralized matrix [11, 12], which can be expected to obtain an optimal GBR effect in vivo.

In this study, the phase inversion technique is employed to prepare the asymmetric porous membrane and the mechanism is similar to that reported elsewhere [1]. The casting membranes are "dried" and the method is named Dry Inversion Method, or are precipitated and the method is named Wet Inversion Method. The solvent starts to vaporize after the slurry casting on the glass plate, the solvent (ethanol) on the surface of the liquid film formed by PA66 or nHA/PA66 composite slurry vaporizes faster than that of inside, then the concentration of PA66 or nHA/PA66 (PA66 preponderance) increases quickly to form the layer which is shaped by means of the colloid particle. Vaporization of the solvent slows down inside the system after the relative compact surface layer (micropore layer) formed. The homogeneous slurry system is disturbed along with the solvent vaporization and results in the phase separation. Part of solvent separates from the homogeneous slurry to form the liquid drop of spread phase, which is called poor PA66 or composite phase. Composite, especially PA66 gathers round the liquid drop to form the continuous phase, which is called rich PA66 or composite phase. After the ethanol gradually vaporizes, the porous structure of membrane is solidified through the rich PA66 or composite phase and the macropores or micropores are formed by the poor PA66 or composite phase. The pore size of the membrane depends on the kinetics of droplet growth of poor PA66 or composite phase. The droplet growth is dependent upon among other things, the local polymer concentration. The concentration profile is existed across the thickness of the casting membranes due to the solvent on the exposed surface evaporate faster than that of interior. Thus the droplets near the exposed surface will be small than those far from the exposed surface because of the combination of slower droplet growth rate and shorter growth time [32]. So, novel composite GBR membranes with asymmetric porous structure were obtained.

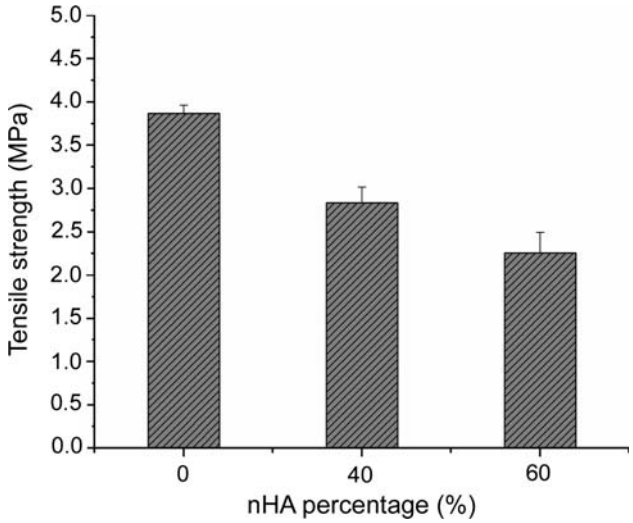

Fig. 6 The tensile strength of PA66, nHA/PA66-40 and nHA/PA66-60 membranes

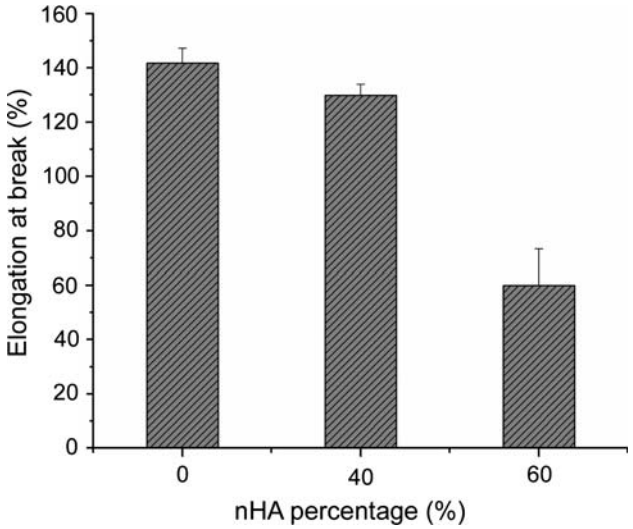

Fig. 7 The elongation at break of PA66, nHA/PA66-40 and nHA/PA66-60 membranes

3.4 Mechanical properties of the membranes

Tensile strength and elongation at break are shown in Figs. 6 and 7 respectively. Both the tensile strength and the elongation at break decrease with the increase of nHA weight percentage in the membranes, especially, the elongation at break of nHA/PA66-60 membrane reduces most greatly. The incorporation of nHA into the PA66 matrix disturbs the continuous phase of PA66 may be one reason for these results. The porous structure maybe also has influence on the mechanical properties of the membranes and the results will be reported later. The elongation at break and the tensile strength of nHA/PA66-40 membranes reduce slightly, suggesting that nHA/PA66-40 composite membrane has optimal strength and toughness to meet the mechanical requirement of GBR.

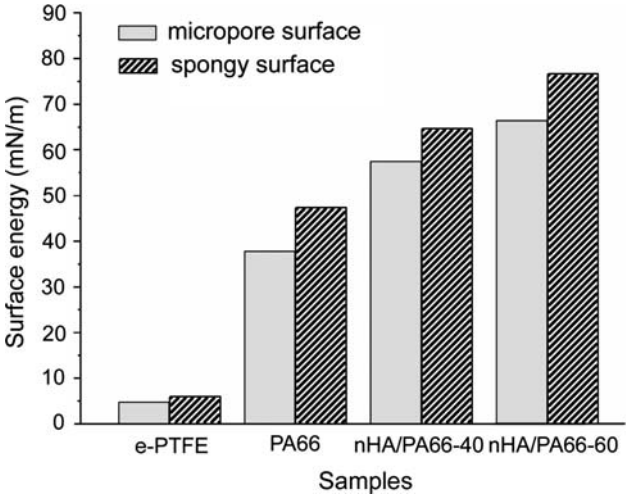

Fig. 8 The surface energy of e-PTFE, PA66, nHA/PA66-40 and nHA/PA66-60 membranes

3.5 Surface energy of the membranes

It can be seen from Fig. 8, the surface energy of PA66, nHA/PA66-40 and nHA/PA66-60 membranes are higher than that of e-PTFE membrane, which might result from the abundance of polar groups, such as $–NH_2$, –COOH, –OH, PO_4^{3-}, in PA66 or/and nHA. The contact angle (data not show here) and surface energy indicate that the e-PTFE membrane is hydrophobic and both the tow sides of the membrane are almost equal. The surface energy of the two sides of fabricated PA66, nHA/PA66-40 and nHA/PA66-60 membranes are very different, as the fabricated membranes have an asymmetric architecture. The surface energy on the spongy porous surface is much higher than that on the relative compact surface (micropore surface). This phenomenon can be explained like that richer pores and more polar groups exposed on the spongy surface than those on the micropore surface, resulting in better wettability on porous texture side.

Surface energy of both the micropore and spongy side increased with the increase of nHA content in the composite membranes, implying that the incorporation of nHA in PA66 matrix improves the surface energy of PA polymer membrane, so the composite membranes have better hydrophilicity than pure PA66 membrane. Lots of researches presented that higher surface energy and hydrophilicity of biomaterials surface resulted in an increase in cells attachment and proliferation [33–36]. In vitro endothelial cell adhesion experiments showed that, with or without the presence of serum in culture medium, the modified materials with good hydrophilicity dramatically enhanced cell attachment and spreading [34].

Therefore, the rough porous surface with high surface energy of the nHA/PA66 composite membranes may be beneficial to promote cells immobility and differentiation into a mature phenotype producing mineralized matrix.

4 Conclusion

In order to overcome the drawbacks of the guided bone regeneration (GBR) membranes used currently and provide an optimal alternative, a bioactive material of nHA/PA66 composite is employed to develop a novel porous membrane with asymmetric structure for GBR. FT-IR and XRD analysis suggest that chemical bonds are formed between nHA and PA66 both in composite powders and membranes. The cross section of the fabricated membranes shows gradient porous structure, which the pores become bigger from the micropore layer to the spongy layer. The surface energy determination also reveals that the fabricated membranes have asymmetric surface properties on the two sides of the membranes. The incorporation of nHA improves the hydrophilicity of the membranes. The elongation at break and the tensile strength of nHA/PA66-40 suggest that composite membrane has good strength and toughness. The rough porous surface with high surface energy of the nHA/PA66 composite membranes may be beneficial to promote cells immobility and differentiation into a mature phenotype producing mineralized matrix. The biocompatibility, bioactivity, osteoconductivity, asymmetric porous structure, mechanical properties and surface energy of the composite membranes can meet the requirement of GBR technique. These composite membranes can be expected to be an alternative using in GBR fields in the future.

Acknowledgments This work was supported by China 973 fund (No.2007CB936102). The authors would like to thank Mr. Chen Shitu from the Analytical and Testing Center of Sichuan University, China for his help of XRD analysis.

References

1. H. Hua, W. Jie, L. Changsheng, Composites Part B **38**, 311 (2007). doi:10.1016/j.compositesb.2006.05.005
2. S. Nyman, J. Gottlow, T. Karring, J. Clin. Periodontol. **9**, 257 (1982). doi:10.1111/j.1600-051X.1982.tb02065.x
3. K. Gotfredsen, L. Nimb, E. Hjorting-Hansen, Clin. Oral Implants Res. **5**, 83 (1994). doi:10.1034/j.1600-0501.1994.050204.x
4. L. Kostopoulos, T. Karring, Clin. Oral Implants Res. **5**, 75 (1994). doi:10.1034/j.1600-0501.1994.050203.x
5. L. Kostopoulos, T. Karring, Clin. Oral Implants Res. **5**, 66 (1994). doi:10.1034/j.1600-0501.1994.050202.x
6. A.H. Melcher, J. Periodontol. **47**, 256 (1976)
7. C. Dahlin, L. Sennerby, U. Lekholm, A. Lindhe, S. Nyman, Int. J. Oral Maxillofac. Implants **4**, 19 (1989)
8. D. Buser, K. Dula, U. Belser, H.P. Hirt, H. Berthold, Int. J. Periodontics Restorative Dent. **13**, 29 (1993)
9. W.L. Murphy, D.H. Kohn, J. Biomed. Mater. Res. **50**, 50 (2000). doi:10.1002/(SICI)1097-4636(200004)50:1<50::AID-JBM8>3.0.CO;2-F
10. G. Hillmann, A. Steinkamp-Zucht, W. Geurtsen, G. Gross, A. Hoffmann, Biomaterials **23**, 1461 (2002). doi:10.1016/S0142-9612(01)00270-8
11. J.Y. Martin, Z. Schwartz, T.W. Hummert, D.M. Schraub, J. Simpson, J. Lankford et al., J. Biomed. Mater. Res. **29**, 389 (1995). doi:10.1002/jbm.820290314
12. G.Rh Owen, J. Jackson, B. Chehroudi, Biomaterials **26**, 7447 (2005). doi:10.1016/j.biomaterials.2005.05.055
13. N.U. Zitzmann, R. Naef, P. Schärer, Int. J. Oral Maxillofac. Implants **12**, 844 (1997)
14. R.K. Shenck, D. Buser, W.R. Hardwick, C. Dahlin, Int. J. Oral Maxillofac. Implants **9**, 13 (1994)
15. F.C. Lin, D.M. Wang, J.Y. Lai, J. Membr. Sci. **110**, 25 (1996). doi:10.1016/0376-7388(95)00211-1
16. N.J. Nasser, A. Friedman, M. Friedman, E. Moor, Injury **36**, 1460 (2005). doi:10.1016/j.injury.2005.05.015
17. C.H.F. Hämmerle, Clin. Oral Implants Res. **12**, 9 (2001). doi:10.1034/j.1600-0501.2001.012001009.x
18. H. Schliephake, M. Dard, H. Planck, Clin. Oral Impl. Res. Denmark **11**, 230 (2000). doi:10.1034/j.1600-0501.2000.011003230.x
19. K. Ito, K. Nanba, S. Murai, J. Periodontol. **69**, 1229 (1998)
20. X.J. Wang, Y.B. Li, J. Wei, K. de Groot, Biomaterials **23**, 4787 (2002). doi:10.1016/S0142-9612(02)00229-6
21. H.N. Wang, Y.B. Li, Y. Zuo, J.H. Li, S.S. Ma, L. Cheng, Biomaterials **28**, 3338 (2007). doi:10.1016/j.biomaterials.2007.04.014
22. L. Zhang, Y.B. Li, X.J. Wang, J. Wei, J. Mater. Sci. **40**, 107 (2005). doi:10.1007/s10853-005-5693-2
23. X. Zhang, Y.B. Li, Y. Zuo, G.Y. Li, Y.H. Mu, H. Li, Composites Part A **38**, 843 (2007). doi:10.1016/j.compositesa.2006.08.00
24. S. Wu, *Polymer Interface and Adhesion* (Marcel Dekker, New York, 1982)
25. J.V. Rau, S.Nunziante Cesaro, D. Ferro, S.M. Barinov, I.V. Fadeeva, J. Biomed. Mater. Res. Part B Appl. Biomater. **2**, 441 (2004). doi:10.1002/jbm.b.30111
26. R.I. Gibson, W. Bonfield, J. Biomed. Mater. Res. **59**, 697 (2002). doi:10.1002/jbm.10044
27. H. El Feki, J.M. Savariault, A.B. Salah, M. Jemal, Solid State Sci. **2**, 577 (2000). doi:10.1016/S1293-2558(00)01059-1
28. N. Vasanthan, R. Kotek, D.-W. Jung, D. Shin, A.E. Tonelli, Polymer (Guildf) **45**, 4077 (2004). doi:10.1016/j.polymer.2004.03.074
29. X.H. Liu, Q.J. Wu, A. Lars, Polymer (Guildf) **43**, 4967 (2002). doi:10.1016/S0032-3861(02)00331-2
30. Y. Zuo, Y.B. Li, J.D. Li, X. Zhang, H.B. Liao, Y.Y. Wang, Mater. Sci. Eng. A **452–453**, 512 (2007). doi:10.1016/j.msea.2006.11.138
31. L. Cerroni, R. Filocamo, M. Fabbri, C. Piconi, S. Caropreso, S.G. Condo, Biomol. Eng. **19**, 119 (2002). doi:10.1016/S1389-0344(02)00027-8
32. P.M. Atkinson, D.R. Lloyd, J. Membr. Sci. **171**, 1 (2000). doi:10.1016/S0376-7388(99)00376-2
33. R.E. Baier, A.E. Meyer, J.R. Natiella, J. Biomed. Mater. Res. **18**, 337 (1984). doi:10.1002/jbm.820180404
34. S.M. Kuo, S.W. Tsai, Artif. Cells Blood Substit. Immobil. Biotechnol. **25**, 551 (1997)
35. H.B. Lin, W. Sun, D.F. Mosher, C. García-Echeverría, S.L. Cooper, J. Biomed. Mater. Res. **28**, 329 (2004). doi:10.1002/jbm.820280307
36. P. Favia, R. d'Agostino, Surf. Coat Tech. **98**, 1102 (1998). doi:10.1016/S0257-8972(97)00285-5